Journal of Alloys and Compounds 648 (2015) 428–437

Contents lists available at ScienceDirect

Journal of Alloys and Compounds

journal homepage: http://www.elsevier.com/locate/jalcom

Improving tensile properties of dilute Mg-0.27Al-0.13Ca-0.21Mn (at.%) alloy by low temperature high speed extrusion

T. Nakata [a, *], T. Mezaki [a], C. Xu [a], K. Oh-ishi [a], K. Shimizu [b], S. Hanaki [b], S. Kamado [a]

[a] Nagaoka University of Technology, 1603-1, Kamitomioka, Nagaoka 940-2188, Japan
[b] Sankyo Tateyama, Inc., Sankyo Material-Company, 8-3, Nagonoe, Imizu, Toyama 934-8515, Japan

ARTICLE INFO

Article history:
Received 19 May 2015
Received in revised form
28 June 2015
Accepted 6 July 2015
Available online 9 July 2015

Keywords:
High-speed extrusion
Mg–Al–Ca–Mn alloy
Dynamic recrystallization
Texture
Tensile properties

ABSTRACT

As-cast Mg-0.27Al-0.13Ca-0.21Mn (at.%) alloy was extruded at temperatures from 350 °C to 500 °C. We examined the microstructural changes during extrusion at different temperatures to clarify dynamic recrystallization mechanisms during extrusion, and also investigated the effect of extrusion temperature on microstructures and mechanical properties of the alloy. High extrusion exit speed of 60 m/min was successfully achieved at wide range of temperatures from 350 °C to 500 °C even when as-cast dilute Mg-0.27Al-0.13Ca-0.21Mn (at.%) alloy was used as a billet for the extrusion. The extrusion at low temperature refines grain size and weakens basal texture due to continuous dynamic recrystallization (CDRX) together with double twinning. As a result, the alloy sample extruded at 350 °C exhibits higher tensile proof stress of 206 MPa and higher tensile ductility of 29% than T5-treated 6063 aluminum alloy and commercial AZ31 magnesium alloy even in an as-extruded condition. Furthermore, Hall–Petch coefficient for compressive proof stress is 1.8 times larger than that for tensile one, resulting in improvement of yield stress anisotropy (compressive proof stress/tensile yield stress ratio).

1. Introduction

Much attention has been paid to wrought Mg alloys due to their possibility of improving fuel efficiencies by weight reduction of transportation vehicles. But, extrusion speeds of conventional Mg alloys are 1/3 to 2/3 slower than Al alloys [1]. This leads to high costs for fabricating Mg alloy products by extrusions. Generally, homogenization treatment is utilized to increase the maximum extrusion speed [2]; however, this is regarded as time-consuming process and also requires high-thermal energy, leading to high productive cost. Recently, it is found that, without any homogenization treatment, the maximum extrusion speed of Mg–Al–Zn alloys could be raised by lowering the Al and Zn contents [3]; however, as expected, reducing contents of the alloying elements decreases the strengths of the alloys [3], and this makes Mg alloys unsuitable for using as structural components. Precipitates have been used to strengthen Mg alloys [4–6], and it is reported that Mg–Al–Ca alloy system shows significant age-hardening by fine precipitates in spite of their low contents of 0.3 at% Al and 0.3 at% Ca [7]. Recent work related to high-speed extrusion of Mg alloy revealed that a dilute Mg-0.27Al-0.13Ca-0.21Mn (at.%) alloy exhibits sufficient extrudability and moderate age-hardening, resulting in high-strengths [8]. From these results, dilute Mg–Al–Ca–Mn alloys are considered as promising materials for achieving both sufficient extrudablitiy and strengths. On the other hand, little work is conducted about dynamic recrystallization (DRX) of dilute Mg alloys [9]; therefore, the relationship between DRX mechanisms and microstructures are unclear in the high-speed extruded dilute Mg alloys. In this study, we carried out high extrusion exit speed of 60 m/min by using as-cast Mg-0.27Al-0.13Ca-0.21Mn (at.%) alloy and examined the microstructural changes during extrusion at temperatures from 350 °C to 500 °C. In addition to clarifying DRX mechanisms during extrusion, we investigated the effect of extrusion temperature on microstructures and mechanical properties of the alloy.

2. Experimental procedure

An alloy ingot having chemical composition of Mg-0.27 (0.30) Al-0.13 (0.21) Ca-0.21 (0.47) Mn (at.% (wt.%)) (hereafter, dilute AXM alloy) and a diameter of 180 mm was prepared by direct-chill (DC) casting. The microstructure of the as-cast alloy sample was observed by a scanning electron microscope (SEM, JEOL JSM7000F)

* Corresponding author.
E-mail address: s123055@stn.nagaokaut.ac.jp (T. Nakata).

http://dx.doi.org/10.1016/j.jallcom.2015.07.051
0925-8388/

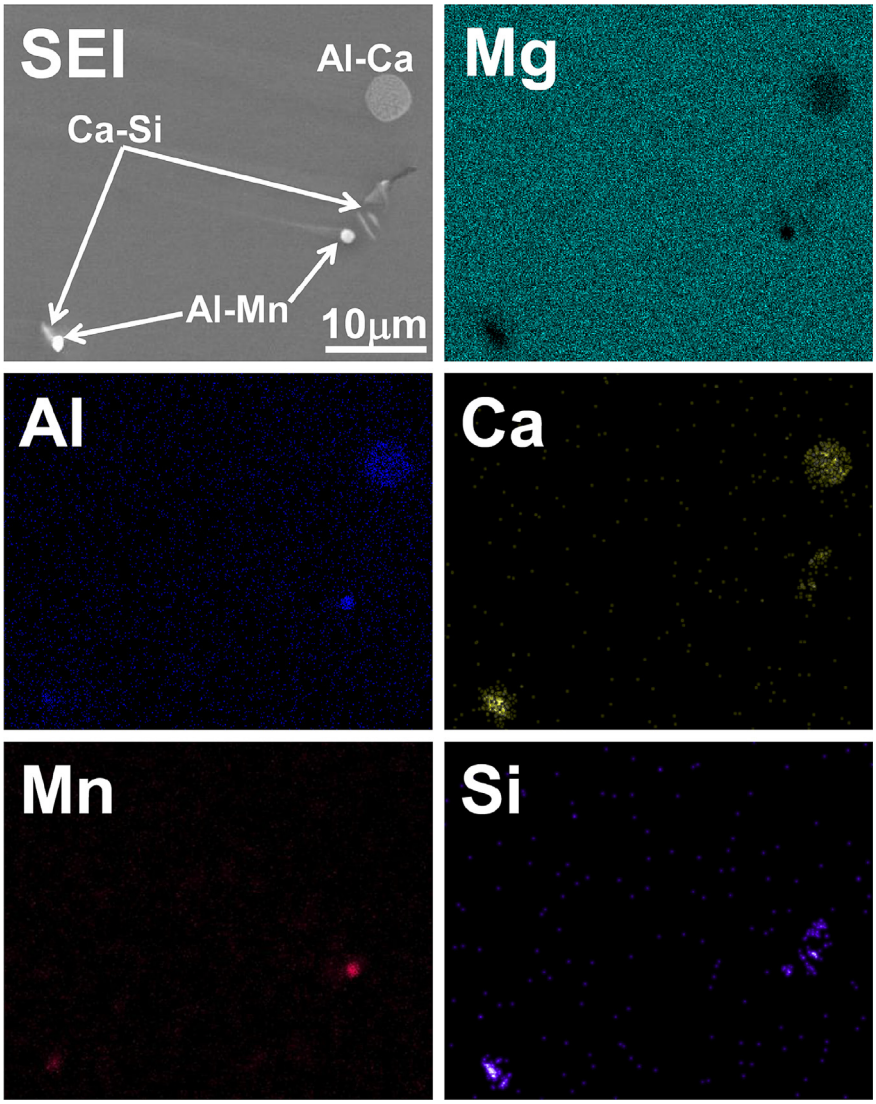

Fig. 1. SEM image and EDS elemental mapping of as-cast Mg-0.27Al-0.13Ca-0.21Mn alloy sample as a billet for extrusion.

equipped with an energy dispersive X-ray spectrometry EDS detector and software. Extrusion was carried out using the as-cast alloy sample (no homogenization treatment) having a diameter of 42.9 mm and a height of 35 mm at 350, 400, 450, and 500 °C at a die-exit speed of 60 m/min with an extrusion ratio of 20. The die used in this study has bearing length of 1.6 mm, bearing angle of 0°, and corner radius of 0.5 mm, and the entrance is a round shape to obtain as-extruded bars with rod shape with 9.6 mm in diameter and about 500 mm in length. After extrusion, the bars were cooled in an atmosphere. Grain sizes and textures of the as-extruded alloy samples were characterized by an electron backscattered diffraction (EBSD) method using a TSL system on the JSM-7000F. Microstructural evolution during extrusion at 350 °C and 500 °C was observed by an optical microscope (OM, VHX2000 KEYENCE) and also by an EBSD method. These observations were conducted by using partially extruded samples (extruded 100 mm in length) at the positions of 5 mm, 10 mm, and 12.5 mm in front of die-entrance. Transmission electron microscope (TEM) observation was performed using JEM-2100F (JEOL) equipped with an EDS software and a detector, and number densities of second-phase particles in the as-extruded alloy samples were evaluated by using convergent-beam electron diffraction method [10]. Mechanical properties of the as-extruded alloy samples were evaluated by both tensile and compressive tests at room temperature under an initial strain rate of 10^{-3} s^{-1} using an AUTO GRAPH AG-I (SHIMADZU). The tensile test specimens were 4 mm in diameter and 22 mm in gage length, and the compressive test specimens were 9.6 mm in diameter and 25 mm in height.

3. Results and discussion

3.1. Microstructure of as-cast sample and extrudability

Fig. 1 shows a SEM image and EDS elemental mapping of the as-cast dilute AXM alloy sample as a billet for extrusion. Only a small amount of compounds consisting of Al and Ca, Al and Mn, or Ca and Si are observed. Moreover, solute segregation, which is often observed in a commercial as-cast AZ alloy [4], is not observed in the as-cast dilute AXM alloy sample, may be due to the low concentration of alloying elements.

Fig. 2 (a) shows the bar surfaces of the dilute AXM alloy samples extruded at the die-exit speed of 60 m/min and at temperatures 350 °C and 500 °C. Both alloy samples show crack-free surfaces despite of the high die-exit speed of 60 m/min. As shown Fig. 2 (b),

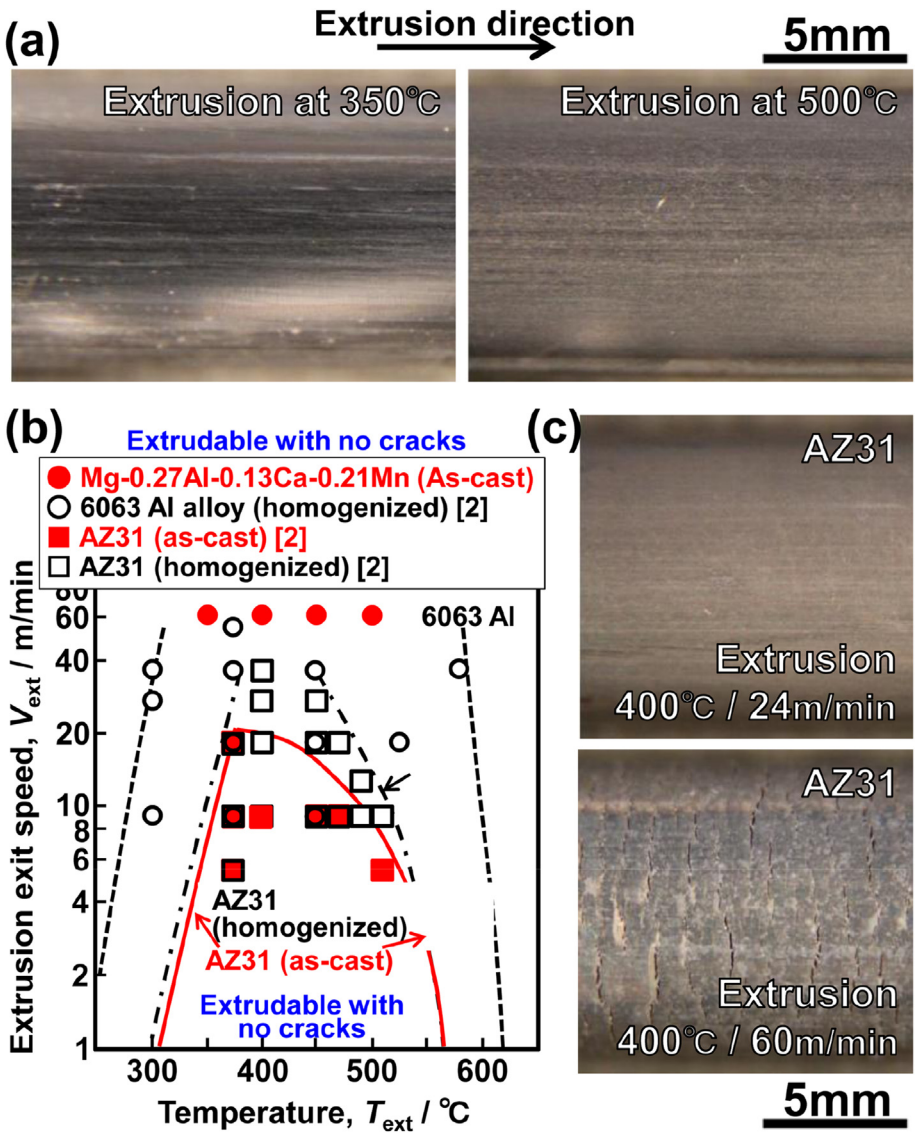

Fig. 2. (a) Bar surfaces of Mg-0.27Al-0.13Ca-0.21Mn alloy samples extruded at 350 °C and 500 °C, (b) Extrusion limit diagram for comparison with commercial AZ31 alloy sample and high-speed extrudable 6063 Al alloy sample, (c) Bar surfaces of AZ31 alloy samples extruded at 400 °C and a die-exit speed of 24 m/min and 60 m/min.

Atwell et al. [2] performed the direct extrusion into 5.4 mm round bar using commercial aluminum and magnesium alloys coated by MoS_2 based dry solid lubricant, a die with a bearing length of 1 mm, a corner radius of 0.25 mm, and a bearing angle of 0° with an extrusion ratio of 30, and reported that a commercial as-cast AZ31 alloy sample can be extruded at a die-exit speed of 20 m/min at the maximum when the extrusion is performed at 375 °C, and extrusion more than 10 m/min of die-exit speed cannot be successfully employed if the extrusion is conducted at 350 °C or 500 °C. Although a homogenization treatment before extrusions can enhance the maximum extrusion speed of the commercial AZ31 alloy sample, low temperature extrusion at 350 °C brings about high extrusion load and high temperature extrusion at 500 °C easily occurs surface cracking if the extrusion speed becomes too high. For these reasons, die-exit speed over 20 m/min cannot be applied for the extrusion at 350 °C and 500 °C even by using the homogenized commercial AZ31 alloy sample [2]. As shown in Fig. 2 (c) that represents bar surfaces of AZ31 (Mg-2.7Al-0.3Zn-0.16Mn, at.%) alloy samples indirectly extruded in our laboratory at 400 °C at a die-exit speed of 24 m/min and 60 m/min using an as-cast sample, the maximum extrudable speed of the as-cast AZ31 alloy sample is almost the same in the case of the direct extrusion reported by Atwell et al. [2]. though the extrusion method is different. This result is mainly attributed to coating of MoS_2 based dry solid lubricant on the billet surface resulting in lower friction and associated lower heat release for direct extrusion [2]. Therefore, the comparison of the extrudability between this work and the Atwell's work is meaningful for emphasizing the good extrudability of the dilute AXM alloy sample As shown in Fig. 2 (a), without any heat-treatment before the extrusion, extrusion at high die-exit speed of 60 m/min is successfully achieved at both low temperature of 350 °C and high temperature of 500 °C indicating the superior extrudability of the as-cast dilute AXM alloy sample. Moreover, the extrudability of the as-cast dilute AXM alloy sample is comparable to that of a homogenized 6063 Al alloy which has best extrudability among Al alloys. This good extrudability of the as-cast dilute AXM alloy sample may be due to the small amount of compounds and little solute segregation even in the as-cast state (Fig. 1).

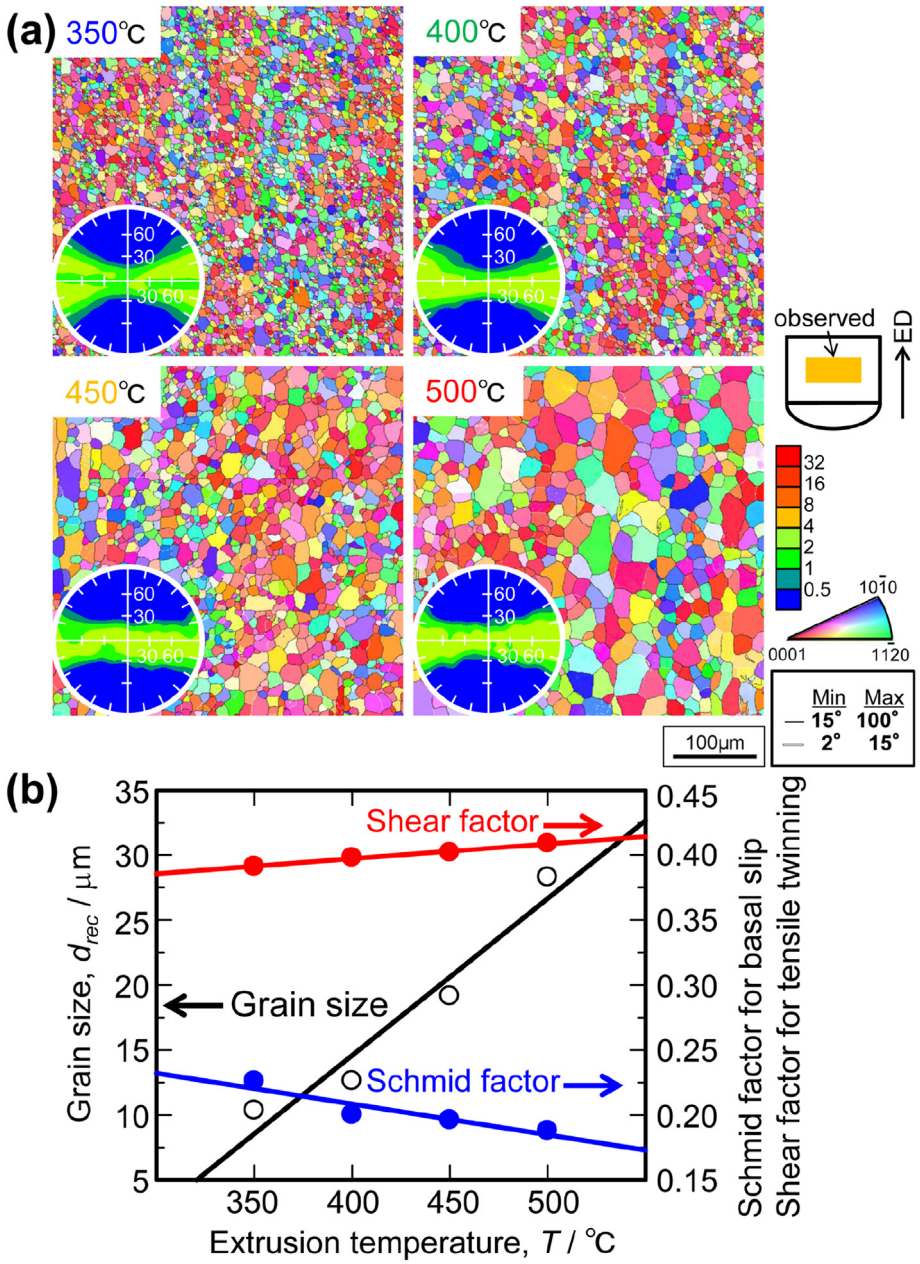

Fig. 3. (a) Inverse pole figure (IPF) maps and (0001) pole figures on central sections parallel to extrusion direction of Mg-0.27Al-0.13Ca-0.21Mn alloy samples extruded at different temperatures, (b) Effect of extrusion temperature on grain size, Schmid factor for basal slip, and shear factor for tensile twinning of as-extruded alloy samples.

3.2. Effect of extrusion temperature on grain sizes, textures, and second-phase particles

Fig. 3 (a) shows inverse pole figure (IPF) maps and (0001) pole figures on the central sections parallel to the extrusion direction of the dilute AXM alloy samples extruded at different temperatures, and Fig. 3 (b) summarizes the effect of extrusion temperature on grain size, Schmid factor for basal slip when an applied tensile load is parallel to the extrusion direction, and shear factor for tensile twinning (meaning Schmid factor for tensile twinning) when an applied compressive load is parallel to the extrusion direction. The grain size is effectively refined by the extrusion at lower temperatures; fine recrystallized grains about 10 μm is obtained by the extrusion at 350 °C. The basal poles of the alloy sample extruded at 350 °C are about 40° away from the transverse direction, while the basal poles of the alloy sample extruded at 500 °C are tilted at about 30° from the transverse direction at the maximum suggesting that the texture intensity becomes weaker with decreasing the extrusion temperature. The texture weakening is also can be seen from the changes of the Schmid factor for basal slip, the Schmid factors for basal slip of the extruded alloy samples increase with decreasing the extrusion temperature; the Schmid factors for basal slip of the alloy sample extruded at 350 °C is 0.22, while that of the alloy sample extruded at 500 °C is 0.18. Hence, it can be said that the basal texture tends to be weakened by extrusion at low temperature. The shear factor for tensile twinning is larger than the Schmid factor for basal slip, and shows the contrary temperature dependence to the Schmid factor for basal slip. However, the changes in the shear factors with decreasing the extrusion temperature are very small.

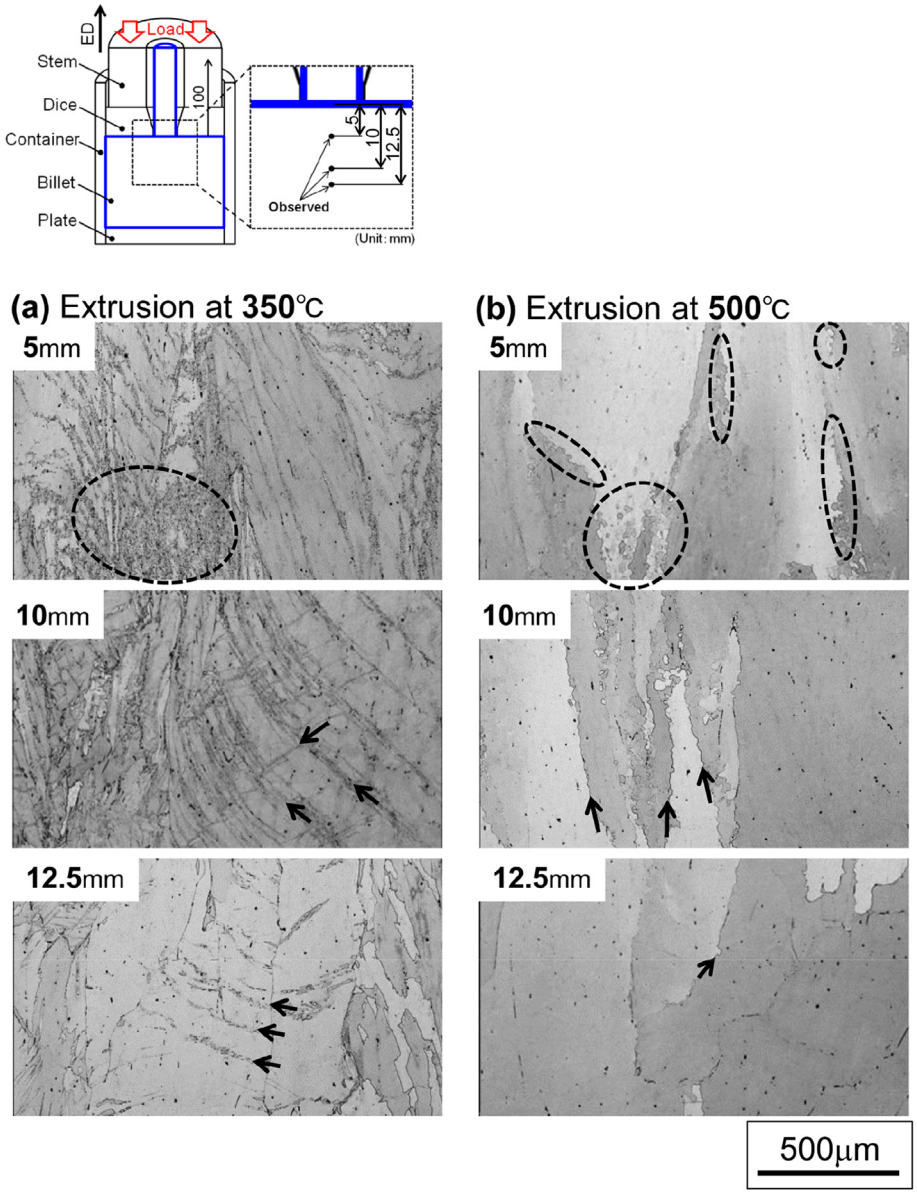

Fig. 4. OM images at positions of 5 mm, 10 mm, and 12.5 mm in front of die-entrance of Mg-0.27Al-0.13Ca-0.21Mn alloy sample partially extruded at (a) 350 °C and (b) 500 °C.

To investigate why the extrusion at low temperature weakens the basal texture, we observed microstructure evolutions during the extrusion at 350 °C and 500 °C. Fig. 4 (a) shows OM images at positions of 5 mm, 10 mm, and 12.5 mm in front of the die-entrance of the alloy sample partially extruded at 350 °C. Thin deformation bands are observed at an initial stage of the extrusion (at 12.5 mm in front of the die-entrance) and fraction of these bands are increased with progress of the extrusion. Fig. 4 (b) shows OM images at positions of 5 mm, 10 mm, and 12.5 mm in front of the die-entrance of the alloy sample partially extruded at 500 °C. The thin deformation bands observed in the alloy sample partially extruded at 350 °C are not observed in the case of the extrusion at 500 °C. On the contrary, initial grain boundaries bulge at the initial stage of the extrusion (at 12.5 mm in front of the die-entrance), and recrystallized grains tend to be formed at the initial grain boundaries. Fig. 5 (a) shows the IPF maps at positions of 10 mm and 12.5 mm in front of die-entrance of the alloy sample partially extruded at 350 °C. The basal planes of the thin deformation bands, which are also observed in the OM images (Fig. 4 (a)), are tilted at about 37° or 30° to the basal plane of the Mg-matrix (at 12.5 mm in front of the die-entrance), suggesting that these bands are formed by occurrences of $\{10\bar{1}1\}$–$\{10\bar{1}2\}$ double twinnings [11,12], and these double twinning areas are divided by low-angle boundaries. At 10 mm in front of the die-entrance, recrystallized grains are observed in the double twinning areas, implying that these grains are formed by continuous DRX (CDRX) during the extrusion at 350 °C [11]. Fig. 5 (b) shows the IPF maps at positions of 10 mm and 12.5 mm in front of the die-entrance of the alloy sample partially extruded at 500 °C. At the initial stage of the extrusion (at 12.5 mm in front of the die-entrance), some grain boundaries bulge as indicated by black arrows and some new recrystallized grains are formed near initial grain boundaries as emphasized by dotted circles. At the next stage of the extrusion (at 10 mm in front of the die-entrance), more new recrystallized grains are nucleated at the initial grain boundaries as highlighted by dotted circles, and these recrystallized grains become larger than the grains at 12.5 mm in front of the die-

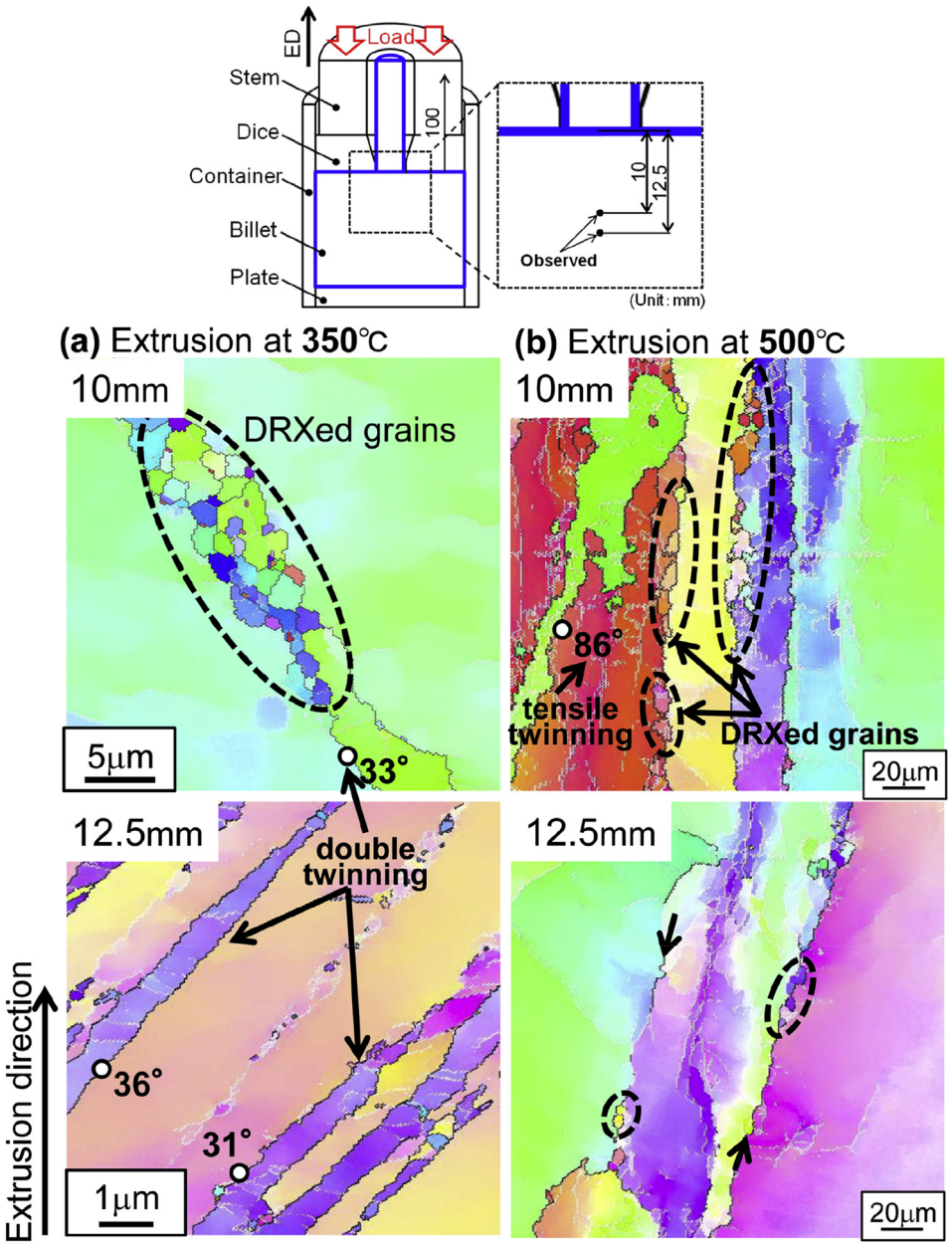

Fig. 5. IPF maps at positions of 10 mm and 12.5 mm in front of die-entrance of Mg-0.27Al-0.13Ca-0.21Mn alloy sample partially extruded at (a) 350 °C and (b) 500 °C.

entrance. Generally, discontinuous DRX (DDRX) grains are developed from initial grain boundaries, and the DDRX grains start growing [13]. Hence, the DDRX near the initial grain boundaries is operative during the extrusion at 500 °C. Although coarse tensile twinning is also observed at 10 mm in front of the die-entrance (Fig. 5 (b)), new recrystallized grains are not formed in the twinnings unlike the extrusion at 350 °C. From these reasons, it can be said that main DRX mechanism during the extrusion at 500 °C is DDRX near the initial grain boundaries. It is reported that the DRXed grains nucleated in shear bands show weak basal texture, while the DRXed grains nucleated by grain boundary bulges exhibit strong basal texture [14,15]. As mentioned in this section, new recrystallized grains during the extrusion at 350 °C are nucleated by CDRX due to formation of shear bands (double twinnings), while the new DDRX grains are mainly formed near the initial grain boundaries during the extrusion at 500 °C. From these facts, the changes in basal textures of the dilute AXM alloy samples extruded at different temperatures are attributed to the DRX mechanism.

Fig. 6 (a) shows the STEM image and STEM-EDS elemental mapping of the dilute AXM alloy samples extruded at 400 °C. Fine second-phase particles distributed within the matrix are composed of Al and Mn as reported in other literature [4,16]. Fig. 6 (b) shows STEM images of the dilute AXM alloy samples extruded at 350 °C and 500 °C. Fine second-phase particles with average diameter of about 15 nm are observed in the alloy sample extruded at 350 °C, while the extrusion at 500 °C forms relatively large second-phase particles of about 39 nm in average diameter. The number density of these particles in the alloy sample extruded at 350 °C is 4.9×10^{20} m^{-3} while that of the alloy sample extruded at 500 °C is only 8.5×10^{19} m^{-3}.

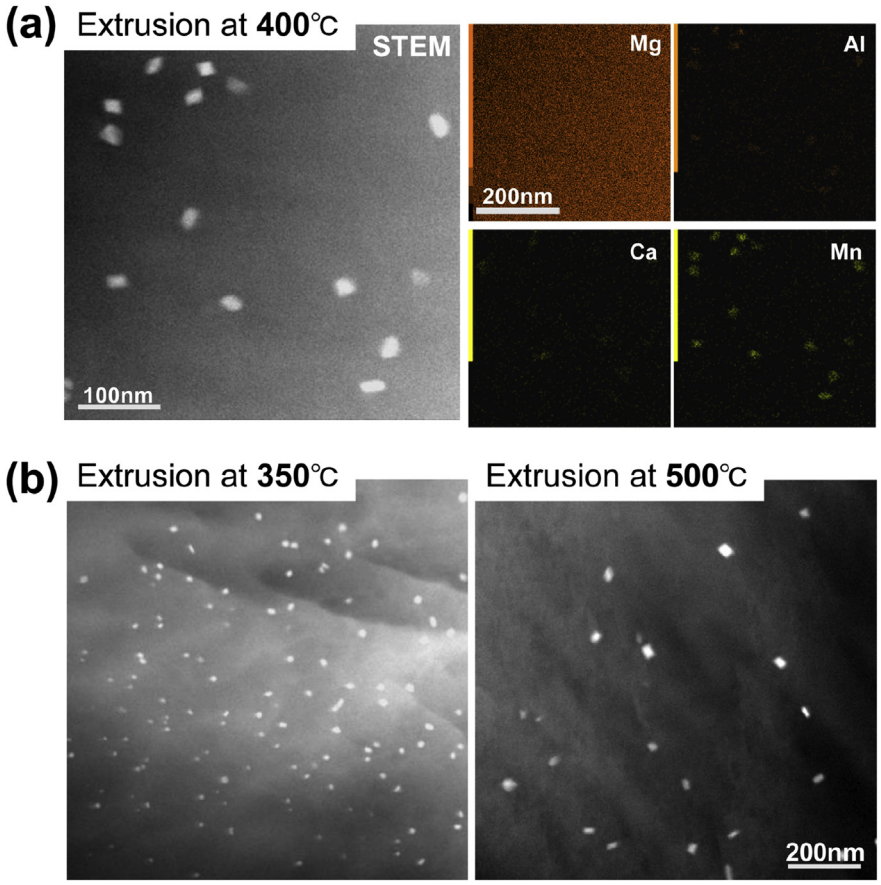

Fig. 6. (a) STEM image and STEM-EDS elemental mapping of Mg-0.27Al-0.13Ca-0.21Mn alloy sample extruded at 400 °C, (b) STEM images of Mg-0.27Al-0.13Ca-0.21Mn alloy samples extruded at 350 °C and 500 °C.

3.3. *Effect of extrusion temperature on mechanical properties*

Fig. 7 (a) shows tensile stress–strain curves of the dilute AXM alloy samples extruded at different temperatures. Both tensile strengths and 0.2% tensile proof stresses (hereafter, TPS) are increased with decreasing the extrusion temperature; the alloy sample extruded at 350 °C exhibits the highest TPS of 206 MPa while the alloy sample extruded at 500 °C shows the lowest TPS of 177 MPa. Low temperature extrusion also enhances the tensile ductility; the alloy sample extruded at 350 °C exhibits the highest tensile ductility of 29%. This high tensile ductility is may be due to the fine grain size and weak basal texture [17–19] as mentioned in Section 3.2. Fig. 7 (b) summarizes the TPS and tensile ductilities of the dilute AXM alloy samples, conventional AZ31 alloy samples extruded at a low extrusion speed of 2.5 m/min and a high extrusion speed of 20 m/min [20], recently developed dilute Mg–Al–Zn–Mn (hereafter, AZ) alloy samples extruded at a high speed of 30 m/min [21], and easily extrudable 6xxx Al alloy samples designed for extrusion products [22]. Note that the conventional AZ31 alloy sample extruded at the high speed of 20 m/min shows lower TPS and tensile ductility than those of the alloy sample extruded at the low speed of 2.5 m/min because the extrusion at high speed coarsens grain sizes of Mg alloys [20,21]. The dilute AXM alloy samples exhibit higher TPS and better tensile ductilities compared to the conventional AZ31 alloy samples and the recently developed dilute AZ alloy samples despite of the higher extrusion speed of 60 m/min, and also show higher TPS than that of T4-treated 6xxx Al alloy samples. In addition, without any aging treatment, the TPS of the dilute AXM alloy samples exceed the T5-treated 6063 Al alloy sample. Furthermore, the dilute AXM alloy sample extruded at 350 °C exhibits comparable TPS as the T6-treated 6063 Al alloy sample in spite of its much higher tensile ductility of 29%. Although the TPS of the T6-treated 6061 Al alloy sample and T5-treated 6005 alloy sample are higher than that of the dilute AXM alloy samples, the tensile ductilities of the dilute AXM alloy samples are higher than those of the both Al alloy samples. Fig. 7 (c) shows compressive stress–strain curves of the dilute AXM alloy samples extruded at different temperatures. The 0.2% compressive proof stress (hereafter, CPS) is improved by the low temperature extrusion as well as the TPS (Fig. 7 (a)), while change in the compressive ductility is little for all the extruded conditions. In spite of convex stress–strain curves in tension, the compression stress–strain curves show concave shape in all the extruded alloy samples. This may be due to the difference of deformation mechanism for tension and compression [23]. Unlike slip dominated flows in tension, twinning becomes dominant mechanism at an initial stage of compression [23–26] when the applied compressive load is parallel to the extrusion direction. The twinning during compression introduces additional barriers to dislocation movement [27], and $\{10\bar{1}2\}$ twinning in Mg reorients the lattice to “hard” crystallographic orientations [25]. Then, transformation of dislocation passing through the twining front induces high hardening rates within the twin interiors [23]. Therefore, the compression curves show concave shape unlike the tension curves.

Generally, proof stresses of metals are increased with decreasing grain sizes, and represented by following equation [28,29]:

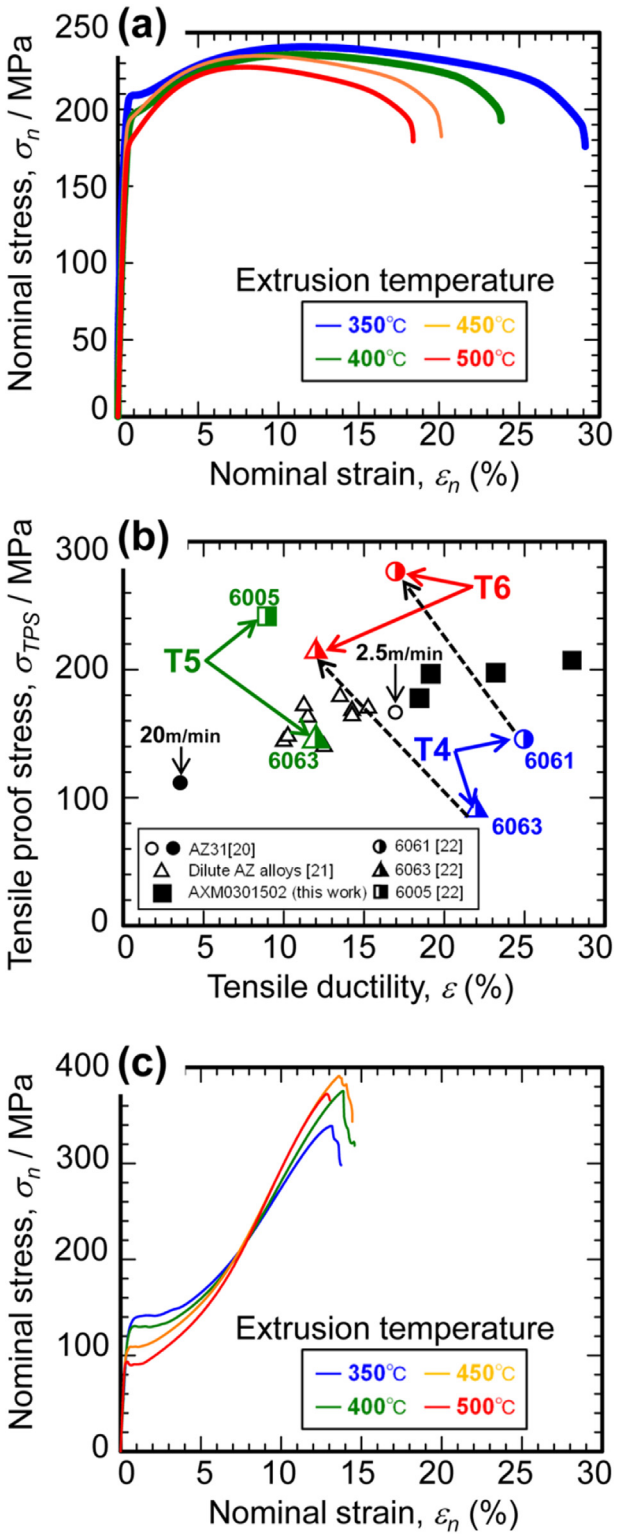

Fig. 7. (a) Tensile stress–strain curves of Mg-0.27Al-0.13Ca-0.21Mn alloy samples extruded at different temperatures, (b) Tensile proof stresses and tensile ductilities of Mg-0.27Al-0.13Ca-0.21Mn alloy samples extruded at 60 m/min, AZ31 alloy samples extruded at 2.5 m/min and 20 m/min, dilute AZ alloy samples extruded at 30 m/min, and high-speed extrudable 6xxx Al alloy samples, (c) Compressive stress–strain curves of Mg-0.27Al-0.13Ca-0.21Mn alloy samples extruded at different temperatures.

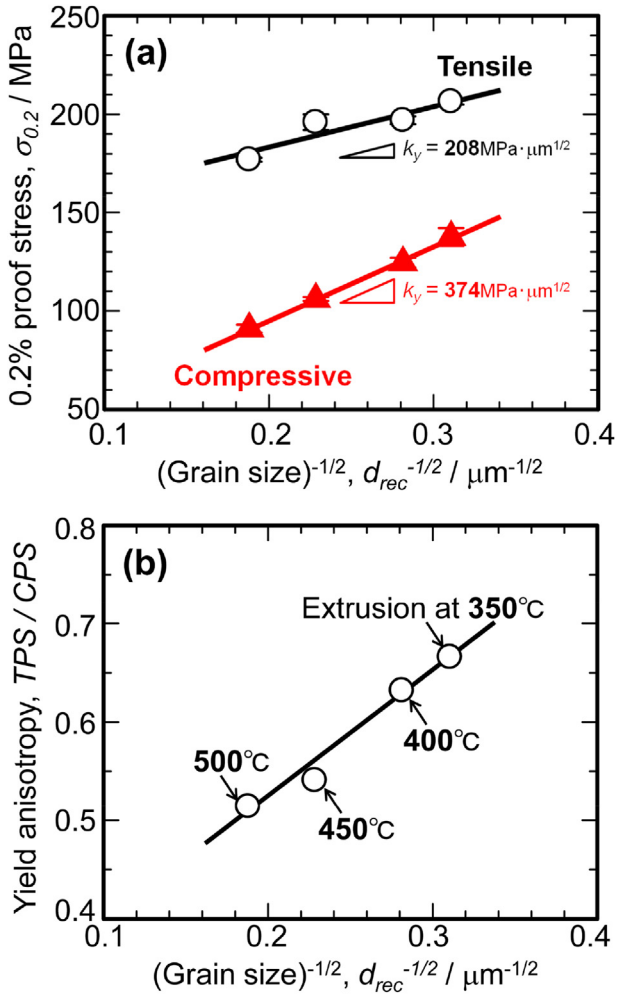

Fig. 8. (a) Tensile and compressive proof stresses versus grain sizes of Mg-0.27Al-0.13Ca-0.21Mn alloy samples extruded at different temperatures, (b) Yield anisotropies versus grain sizes of Mg-0.27Al-0.13Ca-0.21Mn alloy samples extruded at different temperatures.

$$\sigma PS = \sigma 0 + k_y \cdot d^{-1/2} \quad (1)$$

where σ_{PS} is the proof stress, σ_0 is the friction stress for dislocation movement, k_y is the Hall–Petch coefficient, and d is the grain size. The TPS and CPS of the extruded dilute AXM alloy samples obtained in this study are plotted as a function of the inverse square root of the grain size ($d^{-1/2}$) in Fig. 8 (a). Both TPS and CPS are correlated well with the $d^{-1/2}$, and enhanced by grain refining. However, the CPS shows stronger dependence on grain size than the TPS. Similar tendency is also reported in extruded AZ31 alloy samples; Hall–Petch coefficient of the CPS becomes higher than that of the TPS [4,23]. Dominant deformation mechanisms at initial stage of tensile and compressive tests along the extrusion direction are basal or prismatic slip [24,25] and $\{10\bar{1}2\}\langle 10\bar{1}1\rangle$ tensile twinning as expected from Fig. 3 (b) [23,26], respectively, and many metals such as Fe, Cu, Zr, and also Mg show larger grain size dependencies of twinning stress than slip stress [30,31]. Considering these results, it is essential that the CPS has the higher Hall–Petch coefficient than the TPS as shown in Fig. 8 (a).

On the other hand, the proof stress is also influenced by fine precipitates, and fine Al–Mn particles are observed as shown in Fig. 6 (a) and (b). Therefore, we should consider the effect of these

particles on the TPS and CPS. An increase in TPS, $\Delta\sigma_{TPS}$, due to fine precipitates can be estimated by Refs. [4,32]:

$$\Delta\sigma_{TPS} = M\,G\,b \Big/ \{2\,\lambda\,\pi(1-\nu)^{1/2}\} \cdot \ln(dp/b) \quad (2)$$

where M is the inverse of Schmid factor, G is the shear modulus (=15 GPa [4]), b is the magnitude of burgers vector (=0.32 nm [4]), λ is the mean center-to-center spacing between particles, ν is the Poission's ratio (= 0.29 [4]), d_p is the diameter of precipitates. Here, the mean center-to-center spacing between particles, λ, is given as follows [33]:

$$\lambda = d_p \Big/ 2 \cdot \left(3\pi / 2V_f\right)^{1/2} \quad (3)$$

where V_f is the volume fraction of precipitates. Proof stresses of Mg alloys are often related to (0002) basal pole intensity [31,34]; therefore, average Schmid factor for basal slip is used to calculate the $\Delta\sigma_{TPS}$. Table 1 summarizes the related factors for $\Delta\sigma_{TPS}$ and resulting $\Delta\sigma_{TPS}$ for the dilute AXM alloy samples extruded at 350 °C and 500 °C. There is little difference between the alloy samples extruded at 350 °C and 500 °C suggesting that the differences of the TPS of the alloy samples in this study are not the effect of second-phase particles. It is reported that strengths of Mg alloys could be effectively enhanced when fine precipitates with high number density are distributed [35,36]. Although the alloy sample extruded at 350 °C has higher number density of second-phase particles with finer size than that of the alloy sample extruded at 500 °C, the $\Delta\sigma_{TPS}$ of both samples are almost the same. This is considered to be the contribution of stronger basal texture (meaning high value of the inverse of Schmid factor represented by M in Table 1). According to the equation (2), the $\Delta\sigma_{TPS}$ becomes high if the alloy sample has strong basal texture (low Schmid factor for basal slip); therefore, the $\Delta\sigma_{TPS}$ of both alloy samples are not significantly changed in spite of the differences of number density and size of the second-phase particles. In contrast to the TPS, the small volume fraction of these second-phase particles observed in this study cannot prevent $\{10\bar{1}2\}$ $<10\bar{1}1>$ tensile twinning during compression test [4,5]; therefore, the CPS of the dilute AXM alloy samples are not improved by the fine precipitates. For these reasons, the improvements of TPS and CPS by lower temperature extrusions are due to grain refining.

In Fig. 8 (b), the tensile and compressive yield anisotropies (CPS/TPS) of the dilute AXM alloy samples are plotted as a function of the inverse square root of the grain size ($d^{-1/2}$), and it seems that the finer grain size is favorable for eliminating the anisotropy; the alloy sample extruded at 350 °C shows the lowest yield anisotropy (highest CPS/TPS) in all the alloy samples. The yield anisotropy is often observed in Mg alloys especially after wrought process due to formation of strong basal texture and can be eliminated by grain refining [31,37]. The extrusion at lower temperature effectively refines the grain size of the alloy samples in this study; therefore, the dilute AXM alloy sample extruded at 350 °C shows the highest CPS/TPS.

Table 1
Related microstructural factors for $\Delta\sigma_{TPS}$ and resulting $\Delta\sigma_{TPS}$ for the alloy samples extruded at 350 °C and 500 °C.

T_{ext} [°C]	M	d_p [nm]	N_{avy} [m^{-3}]	V_f [%]	λ [nm]	$\Delta\sigma_{TPS}$ [MPa]
350	4.4	15	4.9×10^{20}	0.089	554	28
500	5.3	39	8.5×10^{19}	0.26	829	28

4. Conclusions

The dilute AXM alloy sample is successfully extruded at high die-exit speed of 60 m/min at wide range of extrusion temperatures from 350 °C to 500 °C without any homogenization treatment before extrusion. The as-extruded dilute AXM alloy samples show better tensile properties than those of the commercial AZ31 and dilute AZ alloys. Furthermore, without any aging treatment, the dilute AXM alloy samples exhibit higher tensile properties than the T5-treated 6063 Al alloy. Especially, the dilute AXM alloy sample extruded at lowest temperature of 350 °C shows comparable tensile proof stress of 206 MPa and much higher tensile ductility of 29% as compared to the T6-treated 6063 Al alloy. These attractive tensile properties of the dilute AXM alloy sample extruded at 350 °C are attributed to the fine grains with weak basal texture formed by CDRX with shear bands (double twinning). In addition to the development of high-speed extrudable Mg alloy with high strengths and high ductility, we have revealed the strengthening mechanism for high-speed extruded Mg alloys. The dilute AXM alloy samples form finer grain size with decreasing the extrusion temperature leading to high TPS, CPS. Moreover, it is found that the fine grain size is effective for eliminating the tension and compressive yield anisotropy of the high-speed extruded alloy samples.

Acknowledgment

This work was supported by JSPS KAKENHI Grant Number 25249101 and JST, Advanced Low Carbon Technology Research and Development Program (ALCA), 12102886.

References

[1] F.E. Katrak, J.C. Agarwal, F.C. Brown, M. Loreth, D.L. Chin, in: H.I. Kaplan, J.N. Hryn, B.B. Clow (Eds.), Alternative Ways to Fabricate Magnesium Products, Magnesium Technology 2000, The Minerals & Materials Society (TMS), 2000, pp. 351–354.
[2] D.L. Atwell, M.R. Barnett, Extrusion limits of magnesium alloys, Metall. Mater. Trans. A 38 (2007) 3032–3041.
[3] C. Davis, M. Barnett, Expanding the extrusion limits of wrought magnesium alloys, J. Min. Met. Mater. Soc. (JOM) 56 (Nov 2004) 22–24.
[4] N. Stanford, D. Atwell, The effect of Mn-rich precipitates on the strength of AZ31 extrudates, Metall. Mater. Trans. A 44 (2013) 4830–4843.
[5] J.D. Robson, N. Stanford, M.R. Barnett, Effect of precipitates on slip and twinning in magnesium alloys, Acta Mater. 59 (2011) 1945–1956.
[6] N. Stanford, M.R. Barnett, Effect of particles on the formation of deformation twins in a magnesium-based alloy, Mater. Sci. Eng. A 516 (2009) 226–234.
[7] J. Jayaraj, C.L. Mendis, T. Ohkubo, K. Oh-ishi, K. Hono, Enhanced precipitation hardening of Mg–Ca alloy by Al addition, Scr. Mater. 63 (2010) 831–834.
[8] T. Nakata, T. Mezaki, R. Ajima, C. Xu, K. Oh-ishi, K. Shimizu, S. Hanaki, T.T. Sasaki, K. Hono, S. Kamado, High-speed extrusion of heat-treatable Mg–Al–Ca–Mn alloy, Scr. Mater. 101 (2015) 28–31.
[9] J. Su, S. Kaboli, A.S.H. Kabir, I.H. Jung, S. Yue, Effect of dynamic precipitation and twinning on dynamic recrystallization of micro-alloyed Mg–Al–Ca alloys, Mater. Sci. Eng. A 587 (2013) 27–35.
[10] T. Konno, Principles of TEM image formation (II), Microns. 43 (2008) 212–218.
[11] E. Martin, L. Capolungo, L. Jiang, J.J. Jonas, Variant selection during secondary twinning in Mg-3%Al, Acta Mater. 58 (2010) 3970–3983.
[12] S.W. Xu, S. Kamado, N. Matsumoto, T. Homma, Y. Kojima, Recrystallization mechanism of as-cast AZ91 magnesium alloy during hot compressive deformation, Mater. Sci. Eng. A 527 (2009) 52–60.
[13] F.J. Humphreys, M. Hatherly, Recrystallization and Related Annealing Phenomena Second Edition, Elsevier Society, United Kingdam, UK, 2004, pp. 427–429.
[14] M.R. Barnett, A. Sullivan, N. Stanford, N. Ross, A. Beer, Texture selection mechanism in uniaxially extruded magnesium alloys, Scr. Mater. 63 (2010) 721–724.
[15] A. Sadeghi, M. Hoseini, M. Pekguleryuz, Effect of Sr addition on texture evolution of Mg–3Al–1Zn (AZ31) alloy during extrusion, Mater. Sci. Eng. A 528 (2011) 3096–3104.
[16] S.W. Xu, K. Oh-ishi, S. Kamado, F. Uchida, T. Homma, K. Hono, High-strength extruded Mg–Al–Ca–Mn alloy, Scr. Mater. 65 (2011) 269–272.
[17] J. Koike, T. Miyamura, Microscopic mechanisms of plastic deformation in polycrystalline magnesium alloys, J. Inst. Light Met. 54 (2004) 460–464.
[18] N. Stanford, M.R. Barnett, The origin of “rare earth” texture development in

extruded Mg-based alloys and its effect on tensile ductility, Mater. Sci. Eng. A 496 (2008) 399–408.
[19] S. Sandlobes, S. Zaefferer, I. Schestakow, S. Yi, R.G. Martinez, On the role of non-basal deformation mechanism for the ductility of Mg and Mg–Y alloys, Acta Mater. 59 (2011) 429–439.
[20] T. Murai, S. Matsuoka, S. Miyamoto, Y. Oki, S. Nagao, H. Sano, Effects of zinc and manganese contents on extrudability of Mg–Al–Zn alloys, J. Jpn. Inst. Light Met. 53 (2003) 27–31.
[21] T. Murai, Extrusion of magnesium alloy, J. Jpn. Inst. Light Met. 54 (2001) 472–477.
[22] ASM International Handbook Committee, Metals Handbook, tenth ed., vol. 2, 1990, pp. 100–103.
[23] M.R. Barnett, Z. Keshavarz, A.G. Beer, D. Atwell, Influence of grain size on the compressive deformation of wrought Mg–3Al–1Zn, Acta Mater. 52 (2004) 5093–5103.
[24] Y. Wang, H. Choo, Influence of texture on Hall–Petch relationships in an Mg alloy, Acta Mater. 81 (2014) 83–97.
[25] S.R. Agnew, D.W. Brown, C.N. Tome, Validating a polycrystal model for the elastoplastic response of magnesium alloy AZ31 using in situ neutron diffraction, Acta Mater. 54 (2006) 4841–4852.
[26] M.R. Barnett, Twinning and the ductility of magnesium alloys: part I "Tension" twins, Mater. Sci. Eng. A 464 (2007) 1–7.
[27] I. Karaman, H. Sehitoglu, A.J. Beaudoin, Y.I. Chumlyakov, H.J. Maier, C.N. Tome, Modeling the deformation behavior of Hadfield steel single and polycrystals due to twinning and slip, Acta Mater. 48 (2000) 2031–2047.
[28] G. Sambasivam, Y.V.R.K. Prasad, Grain boundary strengthening in strongly textured magnesium produced by hot rolling, Metall. Trans. A 13 (1982) 2219–2226.
[29] R.W. Armstrong, Theory of the tensile ductile-brittle behavior of polycrystalline h.c.p materials with application to beryllium, Acta Metall. 16 (1968) 347–355.
[30] M.A. Meyers, O. Vohringer, V.A. Lubarda, The onset of twinning in metals: a constitutive description, Acta Mater. 49 (2001) 4025–4039.
[31] J.T. Wang, D.L. Yin, J.Q. Liu, J. Tao, Y.L. Su, X. Zhao, Effect of grain size on mechanical property of Mg–3Al–1Zn alloy, Scr. Mater. 59 (2008) 63–66.
[32] J.F. Nie, Effects of precipitate shape and orientation on dispersion strengthening in magnesium alloys, Scr. Mater. 48 (2003) 1009–1015.
[33] G.L. Roy, J.D. Embury, G. Edward, M.F. Ashby, A model of ductile fracture based on the nucleation and growth of voids, Acta Metall. 29 (1981) 1509–1522.
[34] H. Wang, P.D. Wu, M.A. Gharghouri, Effect of basal texture on mechanical behavior of magnesium alloy AZ31B sheet, Mater. Sci. Eng. A 527 (2010) 3588–3594.
[35] F.R. Elsayed, T.T. Sasaki, C.L. Mendis, T. Ohkubo, K. Hono, Significant enhancement of the age-hardening response in Mg–10Sn–3Al–1Zn alloy by Na microalloying, Scr. Mater. 68 (2013) 797–800.
[36] F.R. Elsayed, T.T. Sasaki, C.L. Mendis, T. Ohkubo, K. Hono, Compositional optimization of Mg–Sn–Al alloys for hinder age hardening response, Mater. Sci. Eng. A 566 (2013) 22–29.
[37] M.R. Barnett, C.H.J. Davies, X. Ma, An analytical constitutive law for twinning dominated flow in magnesium, Scr. Mater. 52 (2005) 623–632.